

Flight Results of the Attitude Determination and Control System for the NEMO-HD Earth Observation Microsatellite

Niels Roth, Bryan Johnston-Lemke, Nicolaas Handoyo, Simon Grocott, Robert E. Zee
Space Flight Laboratory, University of Toronto Institute for Aerospace Studies (SFL)
4925 Dufferin St., Toronto, ON, Canada, M3H 5T6; 1-416-667-7913
nroth@utias-sfl.net

Tomaž Rodič, Ana Urbas, Matevž Bošnjak
Slovenian Centre of Excellence for Space Sciences and Technologies (SPACE-SI)
Askerceva 12, 1000 Ljubljana, Slovenia; +386 1 20 00 444
tomaz.rodic@space.si

ABSTRACT

NEMO-HD is an Earth observation microsatellite designed and built at the Space Flight Laboratory at the University of Toronto Institute for Aerospace Studies (SFL) in collaboration with the Slovenian Centre of Excellence for Space Sciences and Technologies (SPACE-SI) who owns and operates the spacecraft. The mission was launched successfully into a circular Sun-synchronous orbit with 10:30 LT DN at an altitude of 535 km, aboard the VEGA VV16 mission from French Guiana on September 2, 2020. The primary payload is an optical imager, providing still imagery on its panchromatic (PAN) channel with 2.8 m ground sample distance (GSD), 5.6 m GSD on its four multi-spectral channels (R,G,B,NIR), and high definition video with 1920x1080 resolution. To achieve the precise pointing and stability requirements required for high quality optical imagery, the spacecraft is three-axis stabilized using reaction wheels for attitude control, and dual star trackers for attitude determination. The spacecraft has three targeting modes for imaging: inertial pointing, nadir-pointing, and ground target tracking; the exact mode selection depends upon the type of imagery desired. In this paper we discuss spacecraft attitude determination and control system design, and present the detailed attitude determination and control system pointing performance results for the mission in each of the primary operational modes, using one of the two star trackers as the “true” reference attitude.

INTRODUCTION

NEMO-HD is a high-definition, high-resolution Earth monitoring and observation satellite with dual optical payloads. It was designed and built at the University of Toronto Space Flight Laboratory (UTIAS-SFL) in collaboration with the Slovenian Centre of Excellence for Space Sciences and Technologies (SPACE-SI). The NEMO-HD satellite was launched aboard the VEGA VV16 mission from French Guiana on September 2, 2020 (see Figure 1). The satellite has completed its commissioning process and is now returning valuable imagery data.

NEMO-HD is a reasonably compact spacecraft with an octagonal platform and a mass of 65 kg. As seen in Figure 2, the spacecraft is designed around the payload optical bench, which comprises approximately one half of the spacecraft mass. The platform avionics are built upon SFL’s common suite of power system, command and data handling and attitude control hardware to leverage heritage and experience while still enabling higher performance capabilities to support the demands of the payload.¹



Figure 1: VEGA VV16 Launch lifting off September 2, 2020 – Courtesy of Ariane Space.

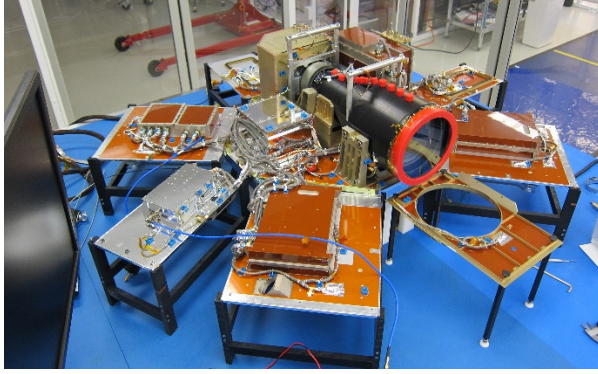


Figure 2: NEMO-HD instrument during integration with the spacecraft.

The primary mission of NEMO-HD is to explore a new Earth observation concept by combining video and multispectral imaging for interactive real time and low latency remote sensing services enabling delivery of pan sharpened multi-spectral images and high definition video products. The primary optical imager provides still imagery with a 10 km swath using a panchromatic (PAN) channel at 2.8 m ground sample distance (GSD) and four multi-spectral channels (R, G, B, NIR) which have 5.6 m GSD. In addition, there are two high definition video channels each with 1920x1080 resolution, one with 2.8 m GSD (5 km swath) and another with 40 m GSD (75 km swath). The layout of these sensors is shown in Figure 3. The four multi-spectral (MS) channels are completely overlaid with one another, while the smaller PAN and HD channels overlap with portions of the MS channels. The PAN channel spans almost the entirety of the MS channels perpendicular to the flight direction (east/west of the ground track), allowing for pan sharpening of the entire MS field of view when operating in swath imaging mode.

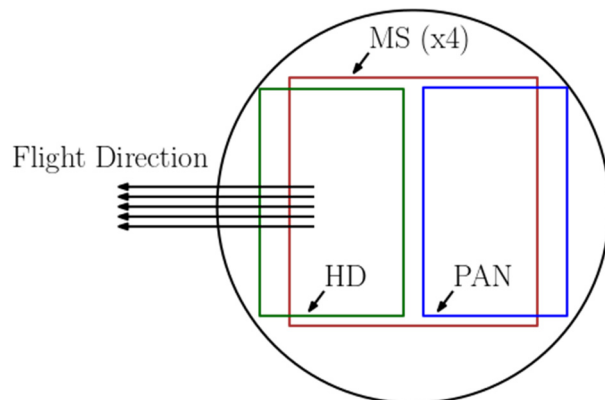


Figure 3: Layout of high-resolution imager fields of view (not to scale). The four MS channels are directly overlaid with one another. The smaller PAN and HD channels overlap with portions of the MS channels, enabling PAN sharpening of the overlapped area.

The NEMO-HD primary optical payload features a 360 mm f/2.3 lens, employing a wideband beam-splitter followed by a focal plane image splitter to accommodate simultaneous capture of 6 sensors in total, 2 CMOS and 4 CCD. The lens has also been designed to have high angular resolution, which allows for the short focal length while still meeting the GSD requirement.

The payload electronics consists of five payload onboard computers (OBCs), one for each still sensor as its high-speed data recorder, connected to a high-speed X-band downlink. In addition two video cameras provide H.264 encoded live video streams, with one camera attached to the primary optics and another to a wide-angle secondary optics.

The primary focus of this paper, however, is to present the attitude determination and control system (ADCS) modes and performance that enable the NEMO-HD instrument to deliver its expected performance.

The paper begins with a description of the hardware complement used in the ADCS design followed by a description of the operating modes of the ADCS system.

Finally, we present the pointing results of seven observation runs demonstrating the three main observation modes: inertial pointing, nadir pointing, and ground target tracking. The results are compared with the pointing requirements for the system which were to achieve 120 arcsec (2σ) in the yaw and pitch axes, and 1000 arcsec (2σ) about the roll axis.

ATTITUDE DETERMINATION AND CONTROL SYSTEM OVERVIEW

In this section we describe the ADCS hardware design. The spacecraft and its coordinate reference frame is shown in Figure 4, for visual reference of hardware positions and orientations.

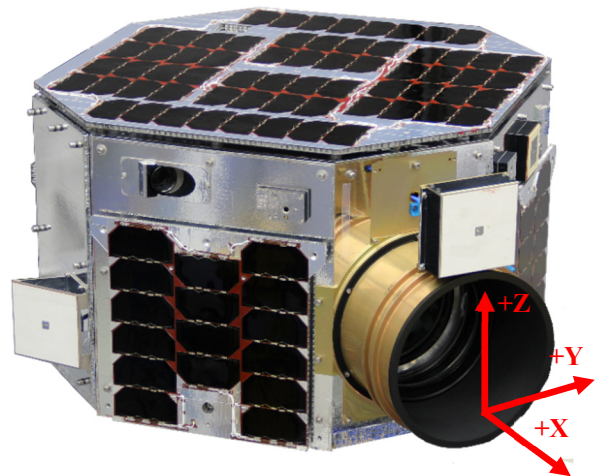


Figure 4: The NEMO-HD spacecraft.

ADCS Sensors

The ADCS sensors fall into two categories: coarse and fine. The coarse sensor suite is comprised of a three axis magnetometer (MAG), six fine sun sensors (FSS), and a three-axis MEMS-based rate sensor (RTS). The fine sensors include a GPS receiver, and a pair of star trackers (STR-A and STR-B).

The magnetometer has two main uses. First, its measurements are used directly in computing the control forces to de-tumble the spacecraft. Second, its vector measurement is used in tandem with the other coarse sensors to compute attitude estimates when the star trackers are not selected for use, or are otherwise unavailable. The magnetometer measurements have an accuracy of about 2° , at the 95% confidence level.

Along with the magnetometer, six fine sun sensors are used to provide a full three-axis attitude solution in sunlight. Four of the sensors are mounted at 45° , 135° , 225° , and 315° in the X/Y plane, with the other two sensors on the $\pm Z$ face. The sensors have a 47° rectangular field of view, and thus provide full coverage of the spacecraft body sphere with some slight overlap between sensors. The sun vector measurements have an accuracy of about 1° , at the 95% confidence level.

The rate sensor is used to help improve the attitude solution during eclipses, when full three-axis solutions are not possible. Based on ground calibration, this sensor has an RMS error of about $0.055^\circ/s$, per axis. The raw rate measurements are dominated by temperature-dependent bias variation, and time-dependent bias drift. The temperature calibration curve is determined from unit-level thermal testing on the ground, while any residual biases due to other sources are determined using an online estimator.

An L1 GPS receiver and antenna system is used for both real time orbit determination and trajectory construction, and to allow recording of raw GPS telemetry for fine position determination on the ground during post-processing. The GPS antenna is mounted opposite the payload boresight, on the $-X$ face, to allow continuous GPS coverage during all spacecraft activities. The accuracy of the onboard solutions is better than 10 m (1σ), with a bias on the order of a 10 m, primarily along the spacecraft radial direction, owing to uncompensated ionospheric errors.⁶

The spacecraft uses two star trackers in order to provide accurate attitude solutions for both real-time pointing, and offline post-processing. The star tracker measurements have a standard deviation of 7.2 arcsec about the pitch/yaw axes, and 64.8 arcsec about the roll axis. The primary reason for the use of two star trackers

was to provide star tracker availability while imaging anywhere within a 30° cone from the sub-satellite point. A Sun exclusion angle of 60° , and Earth limb exclusion angle of 30° were assumed in the design. On the other hand, the minimum separation was bounded below by the 15 arcsec (1σ) determination requirement about the spacecraft pitch/yaw axes. The resulting star tracker orientations are symmetric in the spacecraft body frame: 45° from the $-Z$ axis towards $-X$, and $\pm 30^\circ$ from the X-Z plane, for a total separation of 60° .

ADCS Actuators

There are two sets of ADCS actuators: magnetic torque coils (or magnetorquers), and reaction wheels. There are three orthogonal magnetorquers using a “vacuum-core” design, which provide a control dipole of about 0.92 Am^2 about each body axis. The magnetorquers are primarily used for spacecraft momentum management, and in spacecraft de-tumbling. There are three reaction wheels, providing full three-axis control authority. The wheel axes were selected to lie along the (+X/-Z), (+Y), and (-X/-Z) spacecraft body axes, to provide more uniform momentum and torque control authority over the whole body frame. The wheels have a maximum momentum of about 128 mNms, and a torque authority of about 3 mNm over nearly this whole range. This allows for a maximum slew rate of $1.5^\circ/s$ about an arbitrary spacecraft axis, and provides sufficient control authority for ground target tracking observation modes.

Star Tracker Optimal Measurement Combination

In addition, when both star trackers are available, their solutions can be combined optimally from simultaneous measurements to reduce the attitude determination error as much as possible. The optimal combination algorithm from the GRACE mission is used,² due to its accuracy and computational simplicity. The theoretical accuracy of this approach is computed to second order³ as the inverse of the sum of the inverse covariances for each star tracker. For the star tracker measurement covariances reported for this unit,⁴ and the orientations of the two star trackers onboard, the theoretical error distribution of the combined measurement expressed in the body frame is given by:

$$P_{opt,body} = \left((C_{bs_1} P_s C_{bs_1}^T)^{-1} + (C_{bs_2} P_s C_{bs_2}^T)^{-1} \right)^{-1} \\ = \begin{bmatrix} 63 & 0 & 37 \\ 0 & 34 & 0 \\ 37 & 0 & 63 \end{bmatrix} [\text{arcsec}^2]$$

Onboard, special care is taken to ensure that the star tracker solutions used in the optimal combination have the same time of validity by commanding them simultaneously. This allows the optimal combination to be forced without additional interpolation or attitude

processing. From simulation, a maximum allowable time offset of 100 ms was selected. However, based on onboard telemetry, the solution timestamps are within a few milliseconds of each other, in practice.

For simplicity, the optimal combination weighting matrix is set to a constant value for onboard implementation, whereas ideally the time-varying covariance matrix associated with each star tracker should be used to form the measurement weight. The error incurred in this approximation is not significant for the NEMO-HD mission.

Further to this point, the on-orbit optimal solutions were compared to another method on the ground which uses recursive linear least squares optimization and rigorously accounts for the special properties of direction cosine matrices.³ It was found that the agreement between the two methods is generally on the order of tenths or hundredths of arcseconds, which provides additional confidence in the onboard solution.

ATTITUDE DETERMINATION AND CONTROL MODES

The operational state of the spacecraft from an ADCS perspective is governed by three sets of modes: control, determination, and momentum management. The control mode establishes the spacecraft pointing, the determination mode establishes which sensors to use, and the momentum management mode dictates how the spacecraft angular momentum is regulated. In this section we give an overview of the options within these three classes.

Control Modes

There are four ADCS control modes for the spacecraft: Safe, Passive, B-Dot/Rate Damping, and Three-Axis Control. Generally, transitions between these modes are achieved via time-tagged or direct ground command. Autonomous transitions may also be triggered by the onboard software, in case a software error is detected (e.g., divergence of state estimates), to place the spacecraft into a safe state while allowing ground operators to investigate the error conditions. The main modes and transitions between them are depicted in Figure 5.

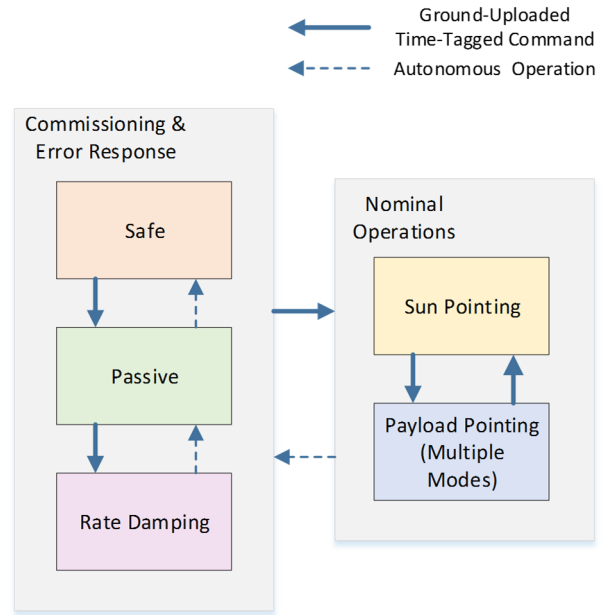


Figure 5: ADCS control modes and mode transitions.

In passive mode, orbit and attitude determination is performed, but no control is commanded. This is primarily a contingency mode, but is also used for initial spacecraft ADCS checkout and calibrations.

In rate damping, or B-Dot mode, the rate of change of magnetic field as measured by the onboard magnetometer is used to compute a set of magnetorquer control commands to reduce spacecraft body rates to roughly two revolutions per orbit. This mode is rarely used outside of initial de-tumbling following deployment from the launch vehicle.⁵

Three-axis control mode is comprised of various “sub-modes”, which encompass all spacecraft pointing options: inertial pointing, ground target tracking, and a general “align/constrain” pointing mode.

The inertial pointing mode controls the spacecraft to a fixed inertial orientation, as specified via ground commanded quaternion. For NEMO-HD, the inertial pointing mode can be used for additional stability during payload observations.

The ground target tracking mode allows a user to specify a set of fixed ground coordinates as a latitude-longitude-altitude triplet, and track this point with a specified body vector while simultaneously constraining a second body vector to orbit normal, local East vector of the ground target, or relative velocity between the spacecraft and ground target. For NEMO-HD, the target tracking mode is used for pointing antennas to the ground for data-downlink, and for imaging operations.

Finally, the align/constrain pointing mode is highly customizable and allows a user to specify: a body vector to point, a pointing option, a body vector to constrain, and a constraint option. The available pointing and constraint options include commonly used vectors such as Sun, orbit normal, nadir, and along-track, as well as custom-specified vectors in the inertial frame or local orbital frame, and alignment or constraint with respect to ground coordinates. For NEMO-HD, custom orbit-frame alignment is used to specify nadir-tracking payload observations, while the custom inertial frame alignment is used for nominal Sun-pointing to maintain a specific beta angle on the main solar array for concurrent maximum power generation and passive spacecraft thermal regulation.

Determination Modes

The three spacecraft determination modes are: Coarse, Fine, and Extra-Fine. Transitions between these modes are specified via ground command. The determination mode controls which attitude sensors are used to estimate the spacecraft attitude state in an extended Kalman filter.

In coarse determination, the magnetometer, fine sun sensors, and rate sensor are used. This yields an attitude determination accuracy better than 5° in sunlight, and better than 10° in eclipse at the 95% confidence level. This determination mode is not suitable for payload pointing operations, but provides adequate accuracy for routine sun-pointing and data download operations.

Fine determination denotes when *only one* star tracker is used to estimate the attitude, whereas extra-fine determination implies the two star tracker optimal measurement combination is used. In the case where extra-fine determination mode is commanded but one star tracker's measurements are not available, the spacecraft falls back to fine. In the case that no star tracker measurements are available, the spacecraft automatically falls back to coarse determination until consistent measurements return.

The nominal determination mode for NEMO-HD is extra-fine, which is commanded for nominal Sun pointing and all payload and data downlink operations.

Momentum Management Modes

Regular momentum management is required to maintain three-axis control authority by preventing reaction wheel saturation as they absorb all the disturbance torques acting on the spacecraft, which for NEMO-HD are primarily due to spacecraft parasitic magnetic dipole, and gravity gradient-induced torques.

There are two momentum management modes used on NEMO-HD, with transitions between them controlled

primarily via ground command. These modes are: off (no momentum management), and inertial.

Inertial momentum management allows a user to specify a target spacecraft angular momentum vector in the inertial reference frame. Then, the magnetorquers are used to regulate the wheel speeds to the required values, with consideration of the current three-axis control mode. The wheel speed regulation and attitude control are concurrent.

Momentum management can also be turned off, to minimize disturbances caused by the relatively noisy magnetic control torques during imaging operations. The momentum management is also disabled for some ADCS calibration procedures.

ADCS COMMISSIONING ACTIVITIES

Prior to beginning mission operations, several ADCS calibration and checkout activities were performed. These include calibration of onboard magnetometer to remove measurement biases due to onboard electronics, calibration of the spacecraft inertia matrix to correct slight offsets from the assumed value due to unmodeled components such as wiring harness, estimation of the spacecraft parasitic magnetic dipole due to unmodeled magnetic components and current loops, star tracker calibration updates to reduce the impact of stray light and improve the solution reliability, and a detailed GPS subsystem checkout.

In addition to these sensor and subsystem level checks, the coarse and fine pointing and determination performance was evaluated on an ongoing basis using both high and low rate on-orbit telemetry.

Star Tracker Relative Orientation Calibration and Exclusion Angles

A calibration of the relative star tracker orientations is required such that the reported attitudes are consistent with each other. This results in smoother transitions when switching between solutions from STR-A alone, STR-B alone, and the optimal quaternion combination. The calibration is formulated as a nonlinear least squares problem, which seeks a set of six offset angles (three per star tracker) to minimize the errors between the body attitudes reported by each star tracker at the same time step. The problem formulation is intentionally under-constrained, because the onboard software requires corrections to each of the nominal body-to-star tracker frames. The cost function is the sum of the two-norms of the 3-2-1 Euler angle error computed between the inertial to body attitude from STR-A and that from STR-B, after applying the calibration adjustments.

The consistency/repeatability of the calibration is evaluated by running the calibration algorithm with several data sets, over a range of targets and operational modes, and assessing the variation in the final solution, considering only three degrees of freedom (i.e., 3-2-1 Euler angle sequence mapping between frame of STR-A and frame of STR-B). Here, the “nominal” relative orientations between star trackers are taken from the spacecraft solid model.

$$\delta C^k = C_{s_2 s_1}^k \cdot C_{s_1 s_2}^{nom} = C_1(\delta\alpha_{1,k})C_2(\delta\alpha_{2,k})C_3(\delta\alpha_{3,k})$$

Running this calibration over eight data sets (from different observations), we obtain the following distribution of relative orientation angles ($\mu \pm 3\sigma$ [arcsec]):

$$\delta\alpha_1 = -426 \pm 23, \delta\alpha_2 = 1089 \pm 11, \delta\alpha_3 = -746 \pm 20.$$

The run-to-run variation in optimized relative orientation is quite low, giving confidence in the overall solution.

In terms of planning star tracker availability during observations, in practice the Earth and Sun exclusion angles are smaller than the design values used. It is found that the exclusion angle for the illuminated Earth limb is 22° , and the Sun exclusion angle is approximately 45° . In fact the star tracker Sun exclusion angle is close to the theoretical limit based on ray tracing through the actual geometric design but an angle above 45° is required for *timely* solutions which can be used as part of the nominal control cycle.

FINE POINTING VERIFICATION

The spacecraft fine pointing verification was performed over a series of observations in three attitude control modes: inertial pointing, nadir tracking, and ground target tracking. In each case, the observation attitudes are planned in advance, using the NORAD TLE to predict targeting times and viewing geometries, however it should be noted that in real-time that output of an orbital EKF based on GPS measurements is used to determine the position of the spacecraft so that targeting is precise. The observation sequence for each target follows a similar profile. Six minutes before the target comes into view, command extra-fine determination mode, disable momentum management, and command the observation attitude. The payload is commanded to take still frame images on the PAN and MS channels one frame per second, resulting in 60 images taken ± 30 s from time of closest approach to the target. The observation attitude is held until three minutes after the time of closest approach, at which point slew to the nominal sun-pointing attitude is commanded.

There were two spacecraft configurations tested, denoted “configuration B” and “configuration C”. In configuration B, both star trackers’ telemetry was recorded, but only STR-A telemetry was used in the onboard feedback control. The pointing control errors are then computed from a post-processed optimal star tracker combination. This allows us to assess the spacecraft control error when only one star tracker is used. In configuration C, both star trackers are used in the onboard feedback control. The attitude and rate control errors are assessed with respect to the online state estimate from the AEKF.

The configuration B targets and observation modes are: Tehran, Iran (Nadir-Tracking), Moscow, Russia (Target Tracking), and Hamburg, Germany (Inertial). The configuration C targets and observation modes are Las Vegas, U.S.A. (Nadir-Tracking), Chicago, U.S.A. (Inertial), Whitehorse, Canada (Target-Tracking), and Frankfurt, Germany (Target-Tracking).

Unless otherwise stated, the control errors are computed over the 60 to 70 second observation timespan for each target. In each case, the control errors presented come from the cumulative distribution function of the attitude and rate control error is evaluated at the 95th percentile. The angular error plots show errors in two ways: first, as 3-2-1 Euler angle error offsets, and second as Euler axis angle error, representing the magnitude of the pointing error.

The target attitudes for each test are constructed as follows:

1. The inertial observation attitude is chosen to be the same as the target tracking attitude with a relative velocity constraint, frozen at the time of closest approach. This selection ensures the target relative motion is almost entirely collinear with the readout direction of the detectors, minimizing angular smear around the time of closest approach.
2. The nadir-tracking observation attitude uses the “align/constrained” formulation to track a fixed offset in the local orbital frame, to point the payload at a fixed angle with respect to the ground track. The roll about boresight is adjusted to ensure the target relative velocity is aligned with the imager readout direction.
3. The target tracking attitude is specified directly by providing ground coordinates (geodetic latitude, longitude, and altitude). The target relative velocity constraint is used to minimize angular smear during imaging.

No specific spacecraft angular momentum management setpoints were designed for any sample target, i.e., wheel

speed profiles were not constructed or planned, due to time constraints during planning.

Tehran – Nadir

The attitude and rate control errors from the onboard controller (which used only STR-A) are shown in Figure 6. The error profile is notably quite a bit noisier than the observations performed using both star trackers. This is a result of the control errors being computed in the spacecraft body frame using only one star tracker, such that the noise in its solution about boresight is mapped into all body axes. If we examine the control error in the reference frame of STR-A (shown in Figure 8), we see that the majority of the noise is in fact about the star tracker boresight. The star tracker measurement noise is within the expected 3σ error bounds, as denoted by the horizontal dashed red line.

Using the on-orbit star tracker data, we can also compute the optimal star tracker combination offline, then use the onboard trajectory to compute the control error with respect to the optimal solution. Doing this, we obtain a control error of (33, 22, 22) arcsec about the body X, Y, Z axes respectively, at the 95th percentile.

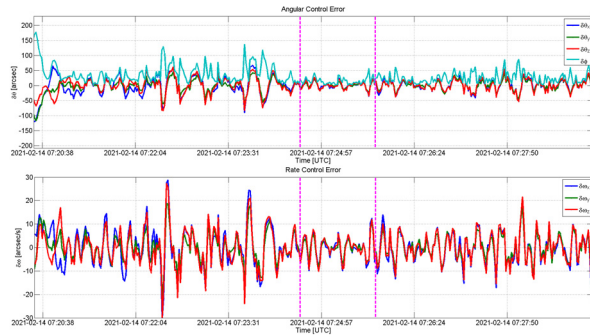


Figure 6: Attitude and rate control error from onboard controller, in spacecraft body frame – Tehran observation. Imaging start and stop denoted by dashed vertical lines.

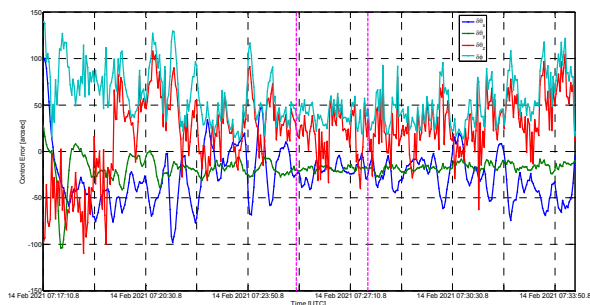


Figure 7: Attitude control error from STR-B, in reference frame of STR-B - Tehran observation.

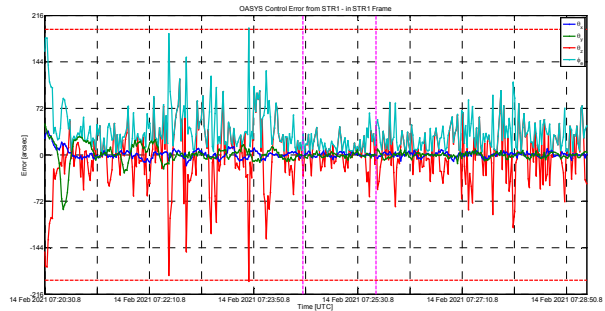


Figure 8: Attitude control error from STR-A, in reference frame of STR-A - Tehran observation. Dashed red lines show star tracker 3σ error in roll determination error.

Moscow – Target Track

The initial transition into the target tracking attitude (not shown) starts at 08:47:48 and ends at 08:50:16. Due to the viewing geometry at this time, both star trackers are obscured by the Earth limb and the spacecraft is initially target tracking with coarse sensors only. At 08:53:40 STR-A solutions return, at which point the control error is about 1400 arcsec. Over the next 30 seconds, the control error converges by an order of magnitude to 164 arcsec. From this point forward, the control error from the Moscow observation is shown in Figure 9. The control error continues to converge in fine determination mode, until the steady-state level is reached at about 08:54:28, or about 48 seconds after first entering fine determination. We find the variation in control error we see is due solely to biased noise about the STR-A boresight. Unfortunately, no useful images are available from this pass due to cloudy weather at the time of imaging.

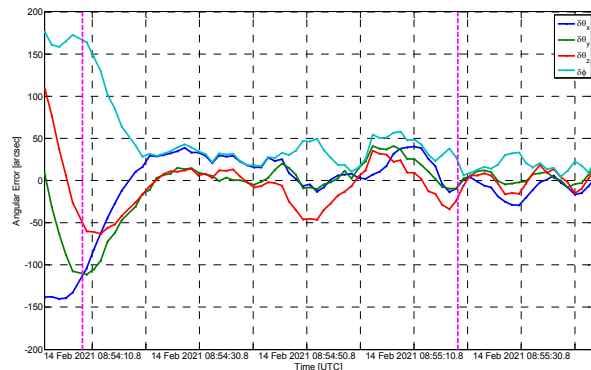


Figure 9: Spacecraft control error from Moscow observation, computed with respect to offline optimal star tracker combination, expressed in spacecraft body frame. Imaging start and stop denoted by dashed vertical lines.

Hamburg – Inertial

With reference to Figure 10, the transition to the inertial imaging attitude over Hamburg is commanded at 10:23:33, and the imaging attitude is achieved at 10:25:35. What follows is a brief period of stabilization, until the steady-state imaging attitude is reached. Throughout this observation, there are noticeable oscillations in control error, mainly coupled about the spacecraft +X/-Z axis. These errors are not due to star tracker determination error, since they appear as known/observable errors in the in the onboard controller and when plotting the control errors in the star tracker reference frames. These control oscillations, whose magnitudes are on the order of 100 to 150 arcsec, appear to be directly related to oscillations in the +X/-Z wheel speed, due to its very low speed throughout this observation. This +X/-Z wheel speed is shown in Figure 11. Here we see six to eight clear disturbances throughout the pass, which correlated directly with control errors observed in the star tracker data. These disturbances are most likely due to the wheel software taking autonomous action to “kick” the wheel in order to improve its internal speed estimate. Such “kicks” are observed visually in lab conditions when commanding the wheel to pass through zero speed at very low torque – exactly the condition during the Hamburg observation. The fact that this wheel was so close to zero speed is a result of no specific spacecraft momentum planning for this observation campaign.

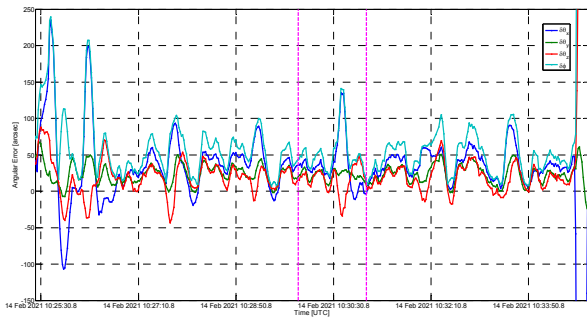


Figure 10: Spacecraft control error from Hamburg observation, computed with respect to offline optimal star tracker combination, expressed in spacecraft body frame. Imaging start and stop denoted by dashed vertical lines.

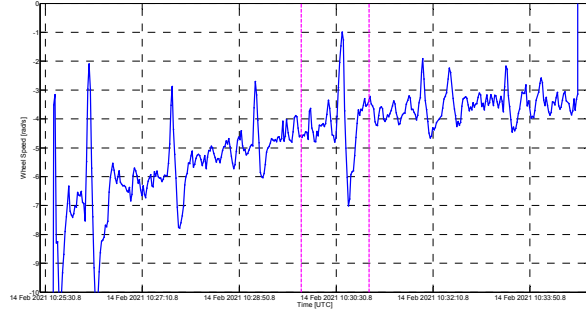


Figure 11: +X/-Z reaction wheel speed from Hamburg observation, showing distinct “kicks” as the wheel forces some rotation to improve its internal speed estimate.

Las Vegas – Nadir

The Las Vegas observation resulted in the best control error of all the tests performed. The attitude and rate control error for this test are shown in Figure 12. The initial maneuver into the observation attitude is commanded at 18:16:53. The spacecraft takes about 2 minutes to reach the target attitude, and the control error takes 40 seconds to settle to a steady state. Leading up to the observation time, we see some minor oscillations in the control error on the order of 7 to 14 arcseconds. These disturbances are a result of inherent controller errors, and from five instances where either STR-A or STR-B did not return a solution on a given cycle. The attitude control error during the observation timespan is better than 10 arcseconds, with rate stability on the order of 1 arcsecond/s.

Two factors leading to the success of this observation are the fact that there were no wheel zero crossings, and the excellent visibility of both star trackers to open sky due to their favourable orientations during nadir-tracking attitudes.

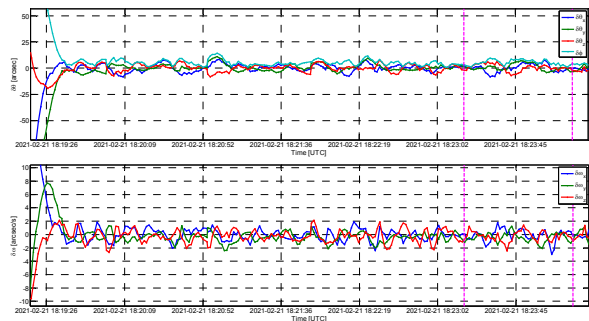


Figure 12: Attitude and angular rate control error from Las Vegas observation, from onboard attitude estimate. Imaging start and stop denoted by dashed vertical lines.

Chicago – Inertial

The attitude and rate control errors as computed from the onboard AEKF solutions are shown in Figure 13. The inertial imaging attitude is commanded at 16:46:44, triggering the onboard software to perform an Euler-axis slew at a fixed rate of 0.7 °/s into the imaging attitude. The slew ends at 16:48:56, which is just before the peak attitude and angular control error on this plot. Less than one minute later at 16:49:44, the control error has converged to better than 5 arcsec per axis. This inertial attitude is regulated for the remainder of the observation. The pointing disturbances leading up to the imaging time are due solely to reaction wheel zero crossing behaviour. The nominal spacecraft momentum vector resulted in a +X/-Z reaction wheel speed less than 5 rad/s. The reaction wheel torque control error at low speeds contributed directly to the X and Z-axis control errors, whose maximum magnitude for this run is about 44 arcsec, with several other local increases in error in the range of 18 to 36 arcsec.



Figure 13: Chicago observation - attitude and angular rate control error. Imaging start and stop denoted by dashed vertical lines.

The one minute imaging timespan is denoted by the dashed vertical lines. At the start of imaging, the control error is still converging from about 25 arcsec following the last reaction wheel-related disturbance. The control error improves steadily throughout the observation, as the reaction wheel is controlled away from 0. Computing the cumulative distribution function of the attitude and rate control errors during the imaging timespan, we find control errors at the 95th percentile of about 26 arcsec and 4.3 arcsec/s.



Figure 14: Image taken during Chicago test observation in the inertial attitude – visibility is poor due to cloud coverage.

Whitehorse – Target Track

The Whitehorse observation represents close to a worst case for target tracking – at the time of closest approach, the target was almost 30 degrees off track (relative to nadir). The attitude and rate control error leading up to and during this observation is shown in Figure 15. The error leading up to the imaging is noticeably poor as compared to other tests, for two reasons. First, due to an unfavourable star tracker orientation during the lead-up to this observation, the controller is using only STR-A from 19:53:55 to 19:58:14 (right before the observation start time). Second, both wheels oriented in the spacecraft X/Z plane undergo zero crossings leading up to this observation, as shown in Figure 16. The net result is pointing disturbances up to about 110 arcsec.

When STR-B solutions return at 19:58:14, there is another disturbance as the spacecraft readjusts its pointing to the new attitude estimate. The adjustment time is about 15 seconds, at which point the control error converges to better than 30 arcsec for the remainder of the observation. An image captured from the PAN channel roughly halfway through the observation window is shown in Figure 17. Qualitatively the image looks quite good; we see several distinctive features of the city, such as roadways, airport runways, trail systems, houses, etc.

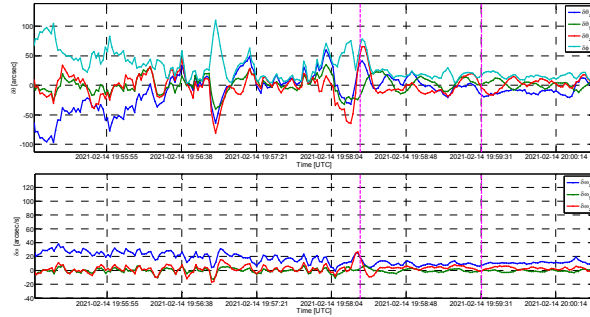


Figure 15: Attitude and rate control error from Whitehorse observation. Imaging start and stop denoted by dashed vertical lines.

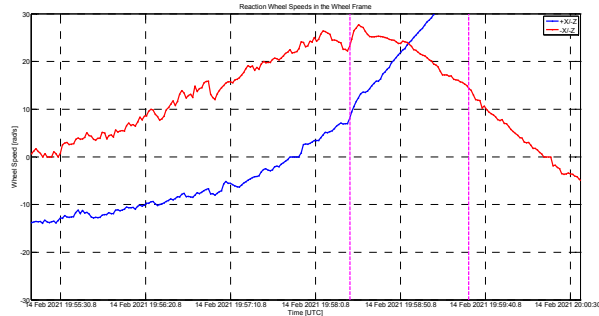


Figure 16: Reaction wheel speeds for +X/-Z and -X/-Z wheels during Whitehorse observation.

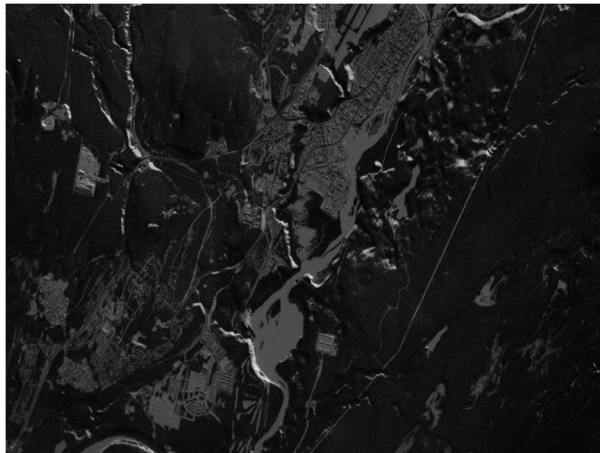


Figure 17: Image taken during the Whitehorse test observation in the ground target tracking attitude.

Frankfurt Airport – Target Track

This observation was not part of the dedicated fine pointing verification tests, but is included as an example of platform pointing stability during HD video imaging. The observation was performed on March 6 2021 around 10:26 UTC, in the ground target tracking attitude.

The spacecraft is initially commanded to the target tracking attitude at about 10:20:29. Due to the satellite-to-target viewing geometry, both star trackers end up obscured by the Earth limb and we drop to coarse determination near the end of the slew to the target attitude. At 10:24:30 the STR-A solution returns, and at 10:24:58 the STR-B solution returns. The control error from this point forward is shown in Figure 18. The start of this plot shows the control error still converging following the re-acquisition of the star trackers. We enter extra-fine determination mode at 10:25:04, from which point we see a second period of convergence because there is a slight jump in the attitude solution when switching from two star trackers individually to the optimal combination. The control error then converges to between 18 and 36 arcsec. Around the time of closest approach at 10:25:56, there is a wheel zero crossing for the +X/-Z wheel, which causes the control error to increase in both X and Z axes, and the net control error reaches just under 72 arcsec. The HD video is taken between 10:26:00.8 and 10:26:12.8. The corresponding rate control error for this observation has mean [8.8 -0.3 1.8] arcsec/s and standard deviation [6.8 2.1 4.3] arcsec/s. A sequence of frames of the HD video is shown in Figure 19 to demonstrate the image quality and stability. In the HD video itself, cars can be clearly seen moving along the roadway, and taxiing aircraft are also evident. There is some slight rotation between the start and end frame of the observation, but this is due to the change in viewing geometry throughout the observation.

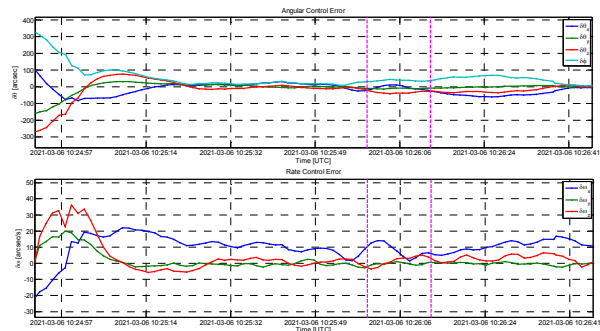


Figure 18: Spacecraft attitude and rate control error during Frankfurt observation. HD video start and stop times denoted by vertical magenta lines.



Figure 19: Sequence of images from Frankfurt airport observation HD video, taken at 0 s, 5 s, and 10 s. Motion is most evident from the translation and rotation of airplanes, and translation of vehicles on the roadway.

FINE POINTING VERIFICATION – SUMMARY

Overall, the fine pointing tests demonstrate that NEMO-HD is exceeding its pointing requirements in all cases. A summary of the attitude and (where available) rate control errors from each test is provided in Table 1. The mission level pointing requirement of 120 arcsec about pitch/yaw and 1200 arcsec about payload boresight is easily achieved in all cases. Leading up to, and during some observations there were control deviations (but within specification) resulting from both reactions wheel zero crossings, and momentary loss of attitude solution due to star tracker outage. In operational practice, it is possible to plan reaction wheel zero crossings, knowing in advance the ground targets, the

desired observation modes, and the imaging times. This should eliminate almost all wheel related pointing errors, whose maximum observed disturbance was 120 arcseconds throughout the test campaign. Star tracker outages cannot be exactly predicted, but the orientation in the body frame ensures that by design at least one star tracker will always be available during imaging almost anywhere on the Earth. Validation of single-startracker pointing error from the “configuration B” tests, show that pointing errors are larger due to the error in determination about star tracker boresight, but still meeting requirements.

We find that the “best” pointing mode is nadir-tracking, owing to constant availability of both star trackers in this imaging attitude, providing the most stable attitude determination and control.

Table 1: Attitude and rate control error summary for fine pointing imaging tests, at the 95th percentile. Mission level requirement of 120 arcsec in pitch/yaw and 1200 arcsec about roll is easily obtained in all cases.

Target	Control Error [arcsec]				Rate Error [arcsec/s]		
	x	y	z	ϕ	x	y	z
Tehran, Nadir, Config. B	33	22	22	45	-	-	-
Moscow, Target Track, Config. B	44	72	56	101	-	-	-
Hamburg, Inertial, Config. B	109	40	40	115	-	-	-
Chicago, Inertial, Config. C	22	5	16	26	3	2	3
Las Vegas, Nadir, Config. C	7	6	6	9	2	2	1
Whitehorse, TT, Config. C	31	22	52	63	14	5	9
Frankfurt, TT, Config. C	57	11	38	66	14	2	5

CONCLUSION

The Attitude Determination and Control System (ADCS) was presented and the performance of three different operating modes, inertial pointing, nadir pointing, and ground target tracking was shown. The pointing results show that the NEMO-HD spacecraft is easily achieving its pointing requirements of 120 arcsec (2σ) in the yaw and pitch axes, and 1000 arcsec (2σ) about the roll axis). Performance varied from 6 – 83 arcsec depending on certain observational complications such reaction wheel zero crossings which we not carefully planned in preparation for the demonstrations. Without zero crossings and availability of both star trackers, both of which can be planned for during regular operations, performance of better than 10 arcsecs during the observation periods has been demonstrably achieved.

Acknowledgments

The primary authors would like to acknowledge the support of the team at SPACE-SI in providing the challenge to achieve an extremely difficult mission and for contracting with SFL to achieve this mission, as well as the hard work and dedication of all SFL staff past and present who helped make this mission a success.

References

1. Larouche, B., Stras, L., Lifshits, J., Grocott, S., Zee, R., Rodič, T., Matko, D., Oštir, K., Peljhan, M., Urbas, A., Fröhlich, H., Blažič, S., Marsetič, A. “NEMO-HD: High Definition High Resolution Global Imaging and Real-Time Video Streaming Satellite,” in *The 4S Symposium 2016*, Valletta, Malta, 2016.
2. Romans, L., “Optimal combination of quaternions from multiple star cameras”, JPL Internal Memorandum, May 2003, url: https://podaac-tools.jpl.nasa.gov/drive/files/allData/grace/docs/quaternion_memo.pdf
3. Barfoot, T.D., *State Estimation for Robotics*, Cambridge University Press, 2017.
4. Enright, J., Sinclair, D., Grant, C.C., McVittie, G. and Dzamba, T., “Towards star tracker only attitude estimation,” in *24th AIAA/USU Conference on Small Satellites*, Logan, Utah, 2010.
5. Stickler, A.C. and K.T. Alfriend, “Elementary Magnetic Attitude Control System,” *Journal of Spacecraft and Rockets*, vol. 13, No. 5, pp. 282-287.
6. Kahr, E., Roth, N. Montenbruck, O., Risi, B. and R.E. Zee, “GPS Relative Navigation for the CanX-4 and CanX-5 Formation-Flying Nanosatellites,”